Carbohydrate Polymers 292 (2022) 119676

Contents lists available at ScienceDirect

Carbohydrate Polymers

journal homepage: www.elsevier.com/locate/carbpol

Chitosan characteristics in electrolyte solutions: Combined molecular dynamics modeling and slender body hydrodynamics

Dawid Lupa [a], Wojciech Płaziński [b,c], Aneta Michna [b,*], Monika Wasilewska [b], Paweł Pomastowski [d], Adrian Gołębiowski [d,e], Bogusław Buszewski [d,e], Zbigniew Adamczyk [b]

[a] M. Smoluchowski Institute of Physics, Jagiellonian University, Łojasiewicza 11, 30-348 Kraków, Poland
[b] Jerzy Haber Institute of Catalysis and Surface Chemistry, Polish Academy of Sciences, Niezapominajek 8, PL-30239 Krakow, Poland
[c] Department of Biopharmacy, Medical University of Lublin, ul. Chodźki 4A, 20-093 Lublin, Poland
[d] Centre for Modern Interdisciplinary Technologies, Nicolaus Copernicus University, Wilenska 4, 87-100 Torun, Poland
[e] Department of Environmental Chemistry and Bioanalytics, Faculty of Chemistry, Nicolaus Copernicus University, Gagarin 7, 87-100 Torun, Poland

ARTICLE INFO

Keywords:
Chitosan molecule conformations
Chitosan molecule charge
Hydrodynamic diameter
Molecular dynamics modeling
Intrinsic viscosity
Zeta potential

ABSTRACT

Molecular dynamics modeling was applied to predict chitosan molecule conformations, the contour length, the gyration radius, the effective cross-section and the density in electrolyte solutions. Using various experimental techniques the diffusion coefficient, the hydrodynamic diameter and the electrophoretic mobility of molecules were determined. This allowed to calculate the zeta potential, the electrokinetic charge and the effective ionization degree of the chitosan molecule as a function of pH and the temperature. The chitosan solution density and zero shear dynamic viscosity were also measured, which enabled to determine the intrinsic viscosity increment. The experimental results were quantitatively interpreted in terms of the slender body hydrodynamics exploiting molecule characteristics derived from the modeling. It is also confirmed that this approach can be successfully used for a proper interpretation of previous literature data obtained under various physicochemical conditions.

1. Introduction

Chitosan is a linear polysaccharide derived from naturally occurring chitin – the second most abundant biopolymer (Kaczmarek et al., 2019) – by its partial deacetylation in enzymatic or base-catalyzed processes. A backbone of chitosan molecule is composed of randomly distributed D-glucosamine (2-amino-2-deoxy-β-D-glucopyranose, deacetylated unit, $GlcNH_2$) and *N*-acetyl-D-glucosamine (2-acetamido-2-deoxy-β-D-glucopyranose, acetylated unit, GlcNAc) linked with β-(1 → 4) bonds, as shown in Fig. 1. Depending on the chitin source and deacetylation process conditions, the molar mass of chitosan varies from 65 to 25,000 kDa (Errington et al., 1993; Morris et al., 2009; Wang et al., 1991).

Among chitosan applications, especially in the biomedical and food context, a tendency to form hydrogel seems to be the most important. Chitosan hydrogels are effective in the targeted adsorption of dyes and proteins from aqueous solutions as was reported by Boardman et al. (2017). Furthermore, chitosan itself has also a high impact on the gelatinization, gel formation, and retrogradation of maize starch as was proved by Raguzzoni et al. (2016).

Because of its biocompatibility, biodegradability and low toxicity, chitosan-based materials have been thoroughly investigated as a component of chitosan-casein hydrophobic peptides nanoparticles, used as soft Pickering emulsifiers (Meng et al., 2022), for application as antimicrobial agents (Chien et al., 2016), in 3D printing of biocompatible scaffolds (Rajabi et al., 2021; Suo et al., 2021) in wound healing (Bano et al., 2019); (Patrulea et al., 2015), in cosmetics and food products as stabilizers (Saha & Bhattacharya, 2010), (Harding et al., 2017), rheology modifier (thickener), in household and commercial products (Pini et al., 2020; Wardy et al., 2014), for producing macroion films in the layer-by-layer processes at various substrates, comprising targeted drug delivery systems based on nanoparticle cores. Chitosan and its derivatives have also gained much attention due to their unusual properties allowing for adsorption and then effective removal of different types of dyes and heavy metal ions (Wan Ngah et al., 2011;

* Corresponding author.
E-mail addresses: dawid.lupa@uj.edu.pl (D. Lupa), wojtek_plazinski@o2.pl (W. Płaziński), aneta.michna@ikifp.edu.pl (A. Michna), monika.wasilewska@ikifp.edu.pl (M. Wasilewska), pomastowski.pawel@gmail.com (P. Pomastowski), adrian.golebiowski@doktorant.umk.pl (A. Gołębiowski), bbusz@umk.pl (B. Buszewski), zbigniew.adamczyk@ikifp.edu.pl (Z. Adamczyk).

https://doi.org/10.1016/j.carbpol.2022.119676
Received 19 March 2022; Received in revised form 11 May 2022; Accepted 27 May 2022
Available online 30 May 2022

Vakili et al., 2014).

The properties of chitosan solutions were widely studied with the aim to evaluate its molar mass distribution (Hasegawa et al., 1994); the radius of gyration and contour length (Cölfen et al., 2001); (Weinhold & Thöming, 2011), persistence lengths (Berth & Dautzenberg, 2002; Morris et al., 2009), the hydrodynamic diameters and the second virial coefficients (Anthonsen et al., 1993; Berth & Dautzenberg, 2002; Errington et al., 1993). Furthermore, it was found that the physicochemical properties of solutions can be modified by controlled chitosan dispersion in various organic acids (Soares et al., 2019).

A plethora of works was devoted to investigations of rheological properties of chitosan solutions, especially the intrinsic viscosity $[\eta]$ under various physicochemical conditions. An analysis of the available experimental data is presented in Fig. S1 in Supporting Information. Many attempts were undertaken in the literature to rationalize these results characterized by a considerable scatter in terms of the empirical Mark-Houwink (MH) relationship connecting the intrinsic viscosity $[\eta]$ with the molar mass, M_p

$$[\eta] = KM_p^a \tag{1}$$

where M_p is expressed in *Da*, K (usually expressed in dL g $^{-1}$) and a (dimensionless) are empirical constants depending on various parameters, primarily on ionic strength and electrolyte composition, pH, the acetylation degree, the temperature, the molar mass range, the stability of the chitosan solutions, aggregation degree etc. A significant scatter of the fitting parameters was reported in the literature, with K varying between 3×10^{-7} to 1.115×10^{-2} dL g $^{-1}$ and a ranging between 0.147 and 1.26 (Kasaai, 2007) or even 1.37 for ionic strength of 0.005 M (Anthonsen et al., 1993). This hinders a proper theoretical interpretation of experimental data and limits the precision of the MH equation often used for a facile molar mass determination, especially of commercial chitosan samples. The parameters of the MH equation reported for different parameters are collected in Fig. S2.

It should also be mentioned that the experimental intrinsic viscosity having the dimension of dL g^{-1} depends on the density of macroion molecules ρ_p. This prohibits its proper physical interpretation in terms of hydrodynamic models, which postulate that the viscosity of dispersion is independent of the particulate matter density. As discussed in recent works (Adamczyk et al., 2018); (Michna et al., 2021), instead of $[\eta]$, the intrinsic viscosity increment $\upsilon_{exp} = \rho_p[\eta]$ (Morris et al., 2009) is the parameter prone to a sound physical interpretation. However, the calculation of υ_{exp} requires the macroion molecule density to be simultaneously determined with the viscosity measurements. Unfortunately, such a procedure was not used in the literature except for the work of Errington et al. (1993).

Therefore, to increase understanding of chitosan molecule behaviour, a more quantitative approach was applied in this work, founded on the combination of molecular dynamics (MD) modeling with low Reynolds number hydrodynamics. Performed calculations furnished various parameters prone to experimental measurements such as the molecule diffusion coefficient, gyration radius and the intrinsic viscosity increment. The obtained theoretical results were used for the interpretation of experimental data acquired using various techniques such as Fourier transform infrared spectroscopy (FTIR), the dynamic light scattering (DLS), micro-electrophoresis (LDV), matrix-assisted laser desorption/ionization coupled to time of flight mass spectrometry (MALDI-TOF/TOF MS), asymmetric flow field-flow fractionation coupled with multi-angle light scattering (AF4-RI-MALS), the optical waveguide lightmode spectroscopy (OWLS) and the zero shear rate dynamic viscosity measurements. As a result, a quantitative information about the physicochemical properties of chitosan molecule such as the chain conformations and length, effective ionization degree and the number of uncompensated charges as a function of pH and the temperature was acquired.

2. Materials and methods

2.1. Materials

Chitosan sample (lot no. 448869) was supplied by Sigma-Aldrich (Poland) in the form of powder. The molar mass (determined by the viscosity method) given by the producer lies in the range of 50 to 190 kg mol^{-1} (kDa) with an average value of 120 kg mol^{-1}. Detailed characterization of obtained chitosan sample is given in Supporting Information.

NaOH and HCl were analytical grade products of Avantor Performance Materials Poland S.A. All reagents were used as received. Pure water of resistivity 18.2 MΩ was obtained using Milli-Q Elix & Simplicity 185 purification system from Millipore SAS Molsheim, France.

2.2. Methods

The solutions of chitosan were prepared by dissolving a proper amount of the powder in 0.01 M HCl. When necessary, the pH of solution was increased using a proper volume of 1 M NaOH by keeping ionic strength at a constant level.

Elemental composition of the chitosan sample, especially the C/N atomic ratio was determined using Thermo Scientific FlashSmart Elemental Analyzer. Additionally, the presence of characteristic moieties and DA value were evaluated using FTIR (FTIR Nicolet 6700 spectrometer, Thermo Scientific). FTIR spectrum was acquired using the classical KBr pellet method.

The molar mass of chitosan was acquired by AF4-RI-MALS and MALDI-TOF/TOF MS analysis.

The distribution of molar mass and radius of gyration was also determined using Postnova AF2000 MultiFlow system (Postnova Analytics GmbH, Landsberg am Lech, Germany). 10 kDa membrane made out of regenerated cellulose and 350 μm spacer were used in this study.

A RI detector PN3150 (Postnova Analytics GmbH, Landsberg am Lech, Germany) was applied for determining particle concentration.

MALS detector PN3621 (Postnova Analytics GmbH, Landsberg am Lech, Germany) collected data at angles from 12° to 164°; the temperature of the detector cell was set to 35 °C with 80% laser ($\lambda = 532$ nm) power. As a carrier liquid, the 0.01 M HCl solution was used (Merck KGaA, Darmstadt, Germany) filtered through a 0.1 μm nylon membrane (Merck Millipore, Warsaw, Poland). The injection volume was 100 μL.

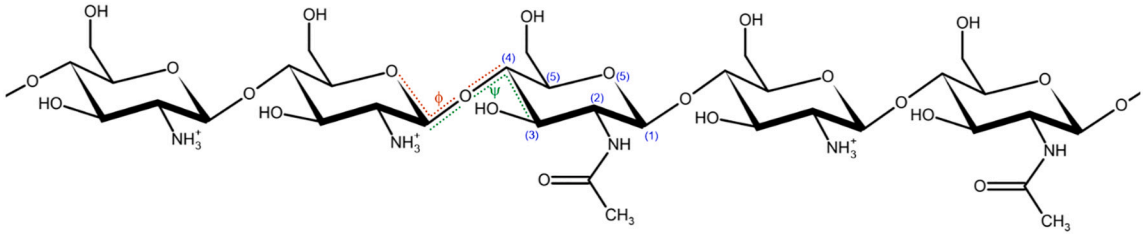

Fig. 1. A schematic representation of the chemical structure of the chitosan molecule with the functionalization motif used in the MD simulations. The acetylation degree (DA) is 40%. The IUPAC-recommended numbering of some atoms and definition of glycosidic dihedral angles are given as well.

All fractionation analyses were performed at room temperature.

The fractionation method was adopted from (González-Espinosa et al., 2019) with some modifications. The detector flow was 0.5 mL min^{-1}. The injection and focusing steps of fractionation consist of 0.2 mL min^{-1} injection, 3.3 mL min^{-1} focusing and 3.0 mL min^{-1} cross-flows through 6 min and then 0.2 min of transition to the elution step. The elution is based on an exponential (0.4) decrease in cross flow to 0.06 mL min^{-1}value. The constant flows were kept to elute all fractions. Evaluation of the data was performed using AF2000 Control software using the Zimm function. Chitosan sample was prepared with a concentration of 2000 mg L^{-1} in 0.01 M HCl, which was dissolved by mixing for at least 2 h. According to (Czechowska-Biskup et al., 2007) $d\eta/dc$ value for chitosan in HCl solution is 0.146 mL g^{-1}.

A MALDI-TOF/TOF MS instrument equipped with a modified neodymium-doped yttrium aluminium garnet (Nd: YAG) laser (1-kHz Smartbeam-II, Bruker Daltonik) operating at the wavelength of 355 nm was used for all measurements. All spectra were acquired in linear positive mode using an acceleration voltage of 25 kV within a m/z range of 30,000 to 500,000 at 50% of laser power and a global attenuator of 30%. All mass spectra were acquired and processed using dedicated software, flexControl and flexAnalysis, respectively (both from Bruker Daltonik).

For MALDI-TOF/TOF MS analysis, chitosan solution was prepared in 0.01 M HCl and 0.1% TFA in water. The analysis was performed using three different matrices – HCCA, DHB and SA. Equal amounts of saturated HCCA solution in TA30 and sample were applied to the plate and allowed to dry. The same protocol was used for DHB (20 mg ml^{-1} in TA30). In contrast, a double layer protocol was used for SA. A saturated solution of SA in EtOH was applied to the plate and allowed to dry. The sample solution and saturated SA in TA30 were then applied to the first layer.

The high-resolution mass spectra of chitosan determined by MALDI-TOF/TOF MS as well as a molar mass distribution, and radius of gyration determined by AF4-RI-MALS were presented in Figs. S6–S8 and Table S3.

The diffusion coefficient and the electrophoretic mobility of chitosan molecules for various pHs were determined using DLS and LDV, respectively. Both DLS and LDV experiments were performed using Malvern Zetasizer Nano ZS apparatus. Chitosan concentration was kept at 100 and 300 mg L^{-1} in the case of the diffusion coefficient and the electrophoretic mobility determination, respectively. The Ohshima (2012) and Einstein (1908) equations were applied to calculate the zeta potentials and the hydrodynamic diameters of chitosan using the electrophoretic mobility and the diffusion coefficient data.

Additionally, the hydrodynamic diameter of chitosan molecules was determined at a low concentration range (typically 5 mg L^{-1} inaccessible to DLS) using the method based on adsorption kinetics measurements in a microfluidic flow cell (for details consult Fig. S12). Accordingly, the chitosan molecule adsorption was measured using the optical wave-guide spectroscopy (OWLS) according to the procedure previously described in Refs. Wasilewska et al. (2019) and Michna et al. (2020). The OWLS 210 instrument (Microvacuum Ltd., Budapest, Hungary) was used. The apparatus is equipped with a laminar slit shear flow cell comprising a silica-coated waveguide (OW2400, Microvacuum). The adsorbing substrates were planar optical waveguides made of a glass substrate (refractive index 1.526) covered by a film of $Si_{0.78}Ti_{0.22}O_2$ (thickness 170 nm, refractive index 1.8). A grating embossed in the substrate enables the light to be coupled into the waveguide layer. The sensor surface was coated with an additional layer (10 nm) of pure SiO_2 according to the previous protocol (Wasilewska et al., 2019). The adsorption kinetic measurements yielded the mass transfer rate of chitosan molecules, which was converted to the diffusion coefficient and in consequence to the hydrodynamic diameter using the Stokes-Einstein relationship (Eqs. S9–S13 in Supporting Information).

The density of chitosan solutions of defined mass fraction (w_p) was determined using the Anton Paar DMA 5000 M densitometer. This apparatus was coupled with the Anton Paar rolling-ball viscometer Lovis 2000 M/ME equipped with a short capillary tube, which allowed simultaneous determination of the dynamic viscosity of solutions with a large precision (0.05%) using relatively small volumes of chitosan solutions (0.1 mL). The zero-shear dynamic viscosity was calculated by extrapolation of dynamic viscosity determined at different shear rates (capillary tilt angles). A description of measurement principles can be found elsewhere (Michna et al., 2021). The measurements were carried out for chitosan mass fractions below 10^{-3} (dilute macroion concentration limit) and at a fixed ionic strength 0.01 M.

All experiments were performed in triplicates.

2.3. Molecular dynamics modeling

A series of chitosan chains of various lengths, composed of 5, 10, 20 and 40 monosaccharide residues (referred to later on as monomers) was considered in the molecular dynamics simulations. The acetylation degree DA of 40% was reflected by the composition of the chains, which contain the periodically repeating motif of functionalization: -$GlcNH_3^+$-$GlcNH_3^+$-GlcNAc-$GlcNH_3^+$-GlcNAc-, see Fig. 1.

The initial configurations of the systems, including the chain solvation as well as the addition of co-ions were created using the CHARMM-GUI online server (Park et al., 2019). The systems of interest consisted of cubic boxes of the initial edge dimensions varying from 4.9 to 21.6 nm, depending on the system. The number of water molecules included in simulation boxes varied from 3800 to 322,500, respectively. The appropriate number of Na^+ and Cl^- ions was added to each system, accounting for its neutral charge and the desired ionic strength value (0.01 M).

The all-atom molecular dynamics (MD) modeling were carried out within the GROMACS 2016.4 package (Abraham et al., 2015). The CHARMM36 force field (Guvench et al., 2011) was used to describe the interactions involving chitosan molecules, accompanied by the CHARMM-compatible explicit TIP3P water model (Jorgensen et al., 1998). According to the assumed pH conditions, all amine groups in the chitosan chain were assumed to be protonated and bear a formal positive charge. The parameters describing the protonated amine moieties were prepared manually and relied on the parameters generated by the *ligand builder* module of the CHARMM-GUI server.

The modeling was carried out applying periodic boundary conditions and in the isothermal-isobaric ensemble. The temperature was maintained close to its reference value (298 K) by applying the V-rescale thermostat (Bussi et al., 2007), whereas for the constant pressure (1 bar, isotropic coordinate scaling) the Parrinello-Rahman barostat (Parrinello & Rahman, 1981) was used with a relaxation time of 0.4 ps. The equations of motion were integrated with a time step of 2 fs using the leap-frog scheme (Hockney, 1970). The hydrogen-containing solute bond lengths were constrained by the application of the LINCS procedure with a relative geometric tolerance of 10^{-4} (Hess, 2008). The full rigidity of the water molecules was enforced by the application of the SETTLE procedure (Miyamoto & Kollman, 1992). The electrostatic interactions were modeled by using the particle-mesh Ewald method (Darden et al., 1998) with a cut-off set to 1.2nm, while van der Waals interactions (LJ potentials) were switched off between 1.0 and 1.2 nm. The translational center-of-mass motion was removed every timestep separately for the solute and the solvent.

The systems were subjected to geometry minimization and MD-based equilibrations in the NPT ensemble, lasting 5–20 ns, depending on the system size. After equilibration, production simulations were carried out for a duration of 100–130 ns and the data were saved to trajectory every 2 ps. The end-to-end, persistence length and gyration radius values were calculated by using the GROMACS routines *gmx polystat* and *gmx mindist*. The anomeric carbon atoms were selected to define the polymer backbone in the case of the longest chain and calculations aimed at persistence length.

The final frames of the equilibration trajectory of the system

containing decameric chains of chitosan were used to initiate enhanced-sampling free energy calculations carried out according to the protocol described below. The calculation of the 2D free energy maps (FEMs) relied on an enhanced-sampling scheme combining parallel tempering (Earl & Deem, 2005) and well-tempered metadynamics (Barducci et al., 2008) as implemented in the PLUMED 2.3 plug-in (Tribello et al., 2014). The well-tempered metadynamics simulations involved a 2D space of collective variables defined by the values of the ϕ and ψ glycosidic dihedral angles. They were defined by the following quadruplets of atoms: ϕ = O_5-C_1-O_1-C'_4, ψ = C_1-O_1-C'_4-C'_3. The parameters of metadynamics were set as follows: initial height of bias portion: 0.1 kJ/mol, bias portion width: 0.314 rad, deposition rate: 0.5 kJ/mol/ps, bias factor (dependent on the ΔT parameter in Eq. (2), ref. (Barducci et al., 2008)): 10. The parallel-tempering relied on 16 metadynamics simulations carried out in parallel at different temperatures ranging from 298.0 to 363.2 K in steps of about 4.3 K, along with replica-exchange attempts performed at 2 ps intervals. All metadynamics simulations were carried out for 10 ns.

3. Results and discussion

3.1. Theoretical modeling results

As mentioned, the calculations were performed for chitosan chains composed of 5, 10, 20 and 40 monomers characterized by the average molar mass 0.179 kg mol^{-1}. The results of this MD modeling enabled to determine the molecule conformation, the time-averaged gyration radius, the end-to-end distance and the extended (contour) length as a function of the degree of polymerization, denoted by *DP*. The derivative parameters such as the persistence length, the extended chain diameter and the molecule density were also theoretically predicted.

Exemplary snapshots of chitosan chain conformations obtained for NaCl concentration of 0.01 M and different polymerization degree are shown in Fig. 2. Qualitatively, one can observe that the chains contain quasi-rigid fragments, but also some kinks, corresponding to reoriented glycosidic linkages. This type of conformation can be traced back to the flexibility of the individual glycosidic linkages between monosaccharides composing the chain, as studied by the additional, metadynamics simulations.

The resulting free energy maps (FEMs, Fig. 3) calculated with respect to the glycosidic dihedral angle values show that the general landscape is roughly independent of the monosaccharide functionalization, i.e. the

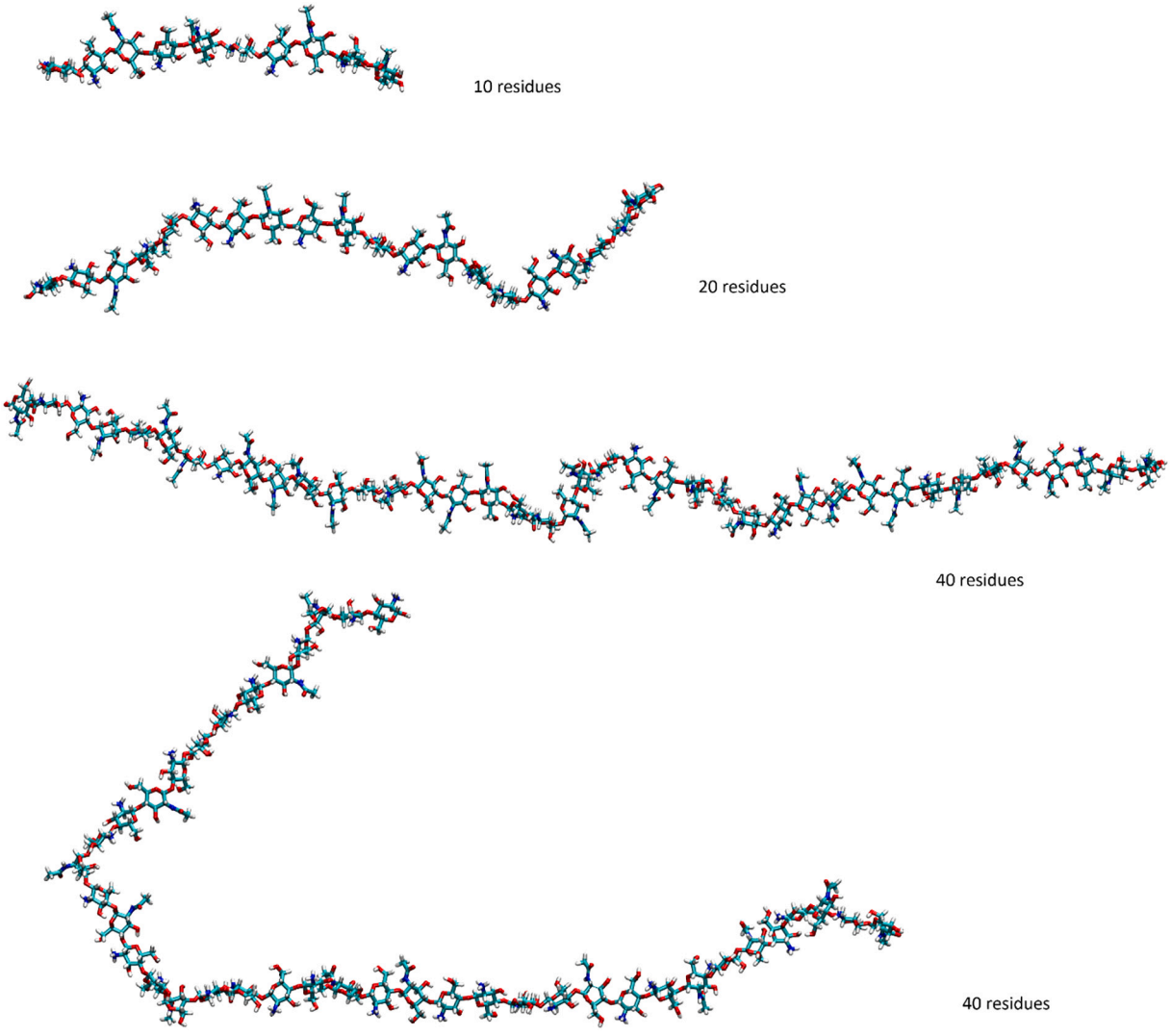

Fig. 2. Snapshots of chitosan chain conformations for systems composed of 10, 20 and 40 residues, derived from MD modeling. Solvent molecules are omitted for clarity, 0.01 M NaCl.

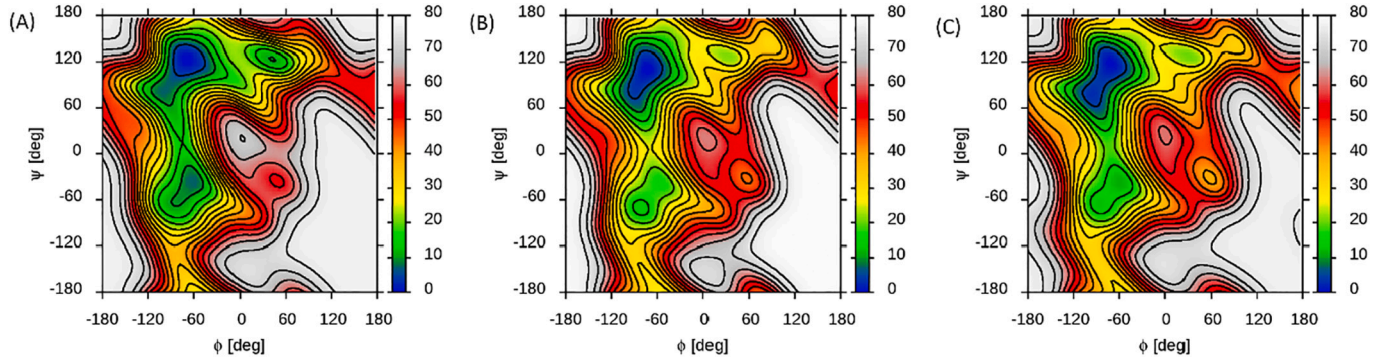

Fig. 3. The free energy maps calculated by metadynamics modeling and illustrating the inherent flexibility of glycosidic linkages between various monosaccharide residues within the chitosan chain: (A) $GlcNH_3^+$-GlcNAc linkage; (B) GlcNAc-$GlcNH_3^+$ linkage; (C) GlcNAc-GlcNAc linkage. ϕ and ψ denote glycosidic dihedral angles, defined according to the IUPAC notation. Energy scale is in [kJ/mol].

location of either the global or local minima on FEM remains unaltered by the substitution of the neighbouring residues. Moreover, the FEM area corresponding to the low (< 5 kJ/mol) free energy levels covers only a narrow fraction of the map, which indicates preferences for a relatively rigid conformation of a given linkage. However, the energy level corresponding to the secondary free energy minima on FEM calculated for the $GlcNH_3^+$- GlcNAc linkage is located close to the zero-level of energy which indicates enhanced flexibility of such linkage, compared to the remaining ones (levels of ca. -7.5 kJ/mol vs. ca. -12 kJ/mol). This corresponds to the population of the alternative chain geometries ca. 5%. Apart from that, an additional, tertiary minimum at the relatively low level of ca. -9 kJ/mol can be observed. Considering the large abundance of this type of linkages and the possible contribution of the remaining linkage types, one has to assume the non-negligible influence of the non-standard conformers of the residue-residue linkage on the overall chain geometry.

The intramolecular hydrogen bonding included mainly interactions between the O_5 ring oxygen atoms and –OH groups of the two consecutive monosaccharide residues. However, the quantitative occurrences of intramolecular hydrogen bonding per 1 residue are low (0.52 per timeframe), indicating the limited intensity of such interaction types and preferred interactions with water molecules instead (6.48 solute-solvent hydrogen bonds per 1 residue). Apart from the conformationally-restricted mutual orientation of the neighbouring residues, no tendency to the formation of regular, helical shapes within a larger dimensional scale was observed.

The MD modeling also allowed to quantitatively determine the time-averaged gyration radius R_g and the average end-to-end distance of the molecule L_{ete} (for 0.01 M HCl) as a function of *DP*. These dependencies are illustrated in Fig. 4. One can observe that these parameters can be well fitted by following linear dependencies

$$R_g = 0.227 + 0.119DP \quad (2)$$

where: R_g is expressed in [nm]

$$L_{ete} = 0.681 + 0.336DP \quad (3)$$

where: L_{ete} is expressed in [nm].

Assuming that *DP* is equal to zero, Eqs. (2) and (3) will provide non-physical results. As the data used to obtain the best-fit parameters were generated for chains of a minimal length of 5 residues, the extrapolation below this value, where end-effects may play a more substantial role, is associated with larger errors of predictions, leading ultimately to non-zero R_g and L_{ete} for $DP = 0$. In spite of that, the relative magnitude of such errors is rather small when referring to the absolute values of both quantities determined for longer chains.

On the other hand, the maximum end-to-end distance, which can be interpreted as the contour length of the fully extended molecule was interpolated by the dependence.

$$L_{ete\ max} = 0.083 + 0.454DP \quad (4)$$

where: $L_{ete\ max}$ is expressed in [nm].

The latter dependence allowed to determine the residue contour length, which was 0.460 nm (see Table 1). Additionally, the persistence length determined during MD simulations and based on the 'backbone' defined by anomeric carbon atoms is 5.0 nm. For comparison, the experimental values reported in the literature vary between 4.5 (Schatz et al., 2003) and 7.6 nm (Lamarque et al., 2005).

The density of the chitosan molecule was calculated using the previously applied method (Adamczyk et al., 2018). Accordingly, the size of the simulation boxes, where a single chitosan molecule was confined, was systematically increased, resulting in the decrease in the chitosan mass fraction from 0.02 to 0. The density of these systems ρ_s, as well as that of the pure solvent ρ_e, were determined in additional MD runs. Then, the dependence of ρ_e/ρ_s on w_p was plotted and fitted by a straight line characterized by the slope s_p and the density was calculated from the formula:

$$\rho_p = \frac{\rho_e}{1 + s_p} \quad (5)$$

Dependences of the relative densities of the chitosan solutions on the mass fraction determined by two complementary approaches: molecular dynamics (MD) modeling and densitometry were presented in Fig. S4, Fig. S5 and Table S2, respectively.

It was determined that, at the temperature of 298 K (0.01 M HCl), the density of the bare chitosan chain (no hydration) was 1.82×10^3 kg m^{-3}. This value can be rescaled upon assumption that each residue in a chain is accompanied by either water molecule(s) (chain hydration) or counterions (ion condensation occurring in the case of charged residues). For instance, the density for the hydrated chain is 1.49×10^3 kg m^{-3} (Table 1). For comparison, the experimental value reported by Errington et al. (Errington et al., 1993) for DA = 58% in 0.2 M NaCl was 1.72×10^3 kg m^{-3}. It should be mentioned that molecule density is the indispensable parameter for a proper hydrodynamic interpretation of the experimentally derived intrinsic viscosity.

Using the densities of 1.82×10^3 kg m^{-3} and 1.49×10^3 kg m^{-3} one can calculate the average volume of a monomer from the dependence $\nu_1 = M_1/(\rho_p N_A)$ which was 0.163 and 0.200 nm^3 for the cases of bare chitosan chain and hydration accompanying one water molecule per residue, respectively (Table 1). Consequently, assuming its cylindrical shape and considering that its molar mass is 0.179 kg mol^{-1}, the equivalent monomer diameter calculated as $d_1 = (4\nu_1/\pi l_m)^{1/2}$ was 0.672 and 0.744 nm, respectively.

Similar values of the extended chain diameter 0.662 and 0.733 nm, for no hydration and hydration with one H_2O molecule per monomer, respectively, were obtained from direct MD modeling. For this purpose,

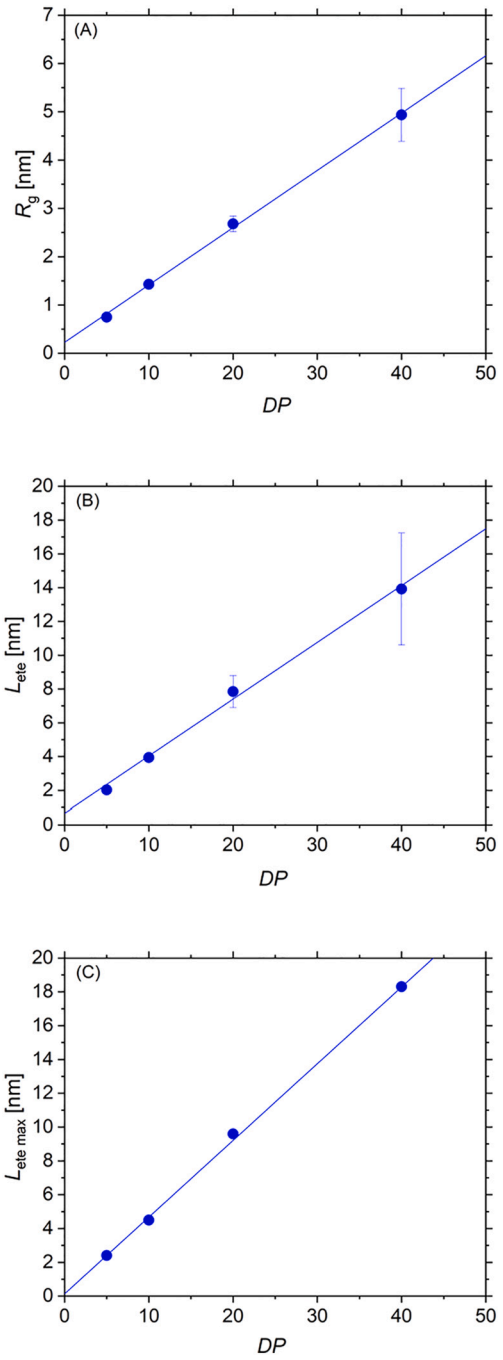

Fig. 4. (A) The average gyration radius (R_g) calculated from the results of MD modeling vs. the degree of polymerization (*DP*) (B) The average end-to-end length (L_{ete}) vs. *DP* (C) The maximal values of the end-to-end length ($L_{ete\ max}$) vs. *DP*. The solid line denotes the linear fitting of theoretical data. Vertical bars in panels (A) and (B) denote the fluctuations of the given quantity found during MD modeling and expressed as standard deviation values.

the density-dependent monomer volume was multiplied by the numbers of mers in the individual chain and related to the monomer length determined for the shortest chain. These data correspond to a negligible ionic strength limit.

On the other hand, for the ionic strength of 0.01 M, the chain diameter was 0.731 and 0.809 nm, for no hydration and hydration, respectively.

The theoretically-determined extended monomer contour length (0.460 nm) agrees reasonably well with the experimental values of 0.49 (Lamarque et al., 2005) and 0.515 nm (Korchagina & Philippova, 2010).

Table 1
Primary physicochemical characteristics of the chitosan molecule derived from MD modeling, 0.01 M HCl, 40% periodic acetylation (DA).

Quantity [unit], symbol	Value	Remarks
Monomer molar mass [kg mol^{-1}], M_1	0.179	Average value for protonated amine groups
Extended monomer contour length [nm], l_m	0.460 ± 0.02	This work, MD modeling, fully extended chain
	0.515	DA = 0.05, (Korchagina & Philippova, 2010)
	0.49	DA = 0.40, (Lamarque et al., 2005)
Persistence length [nm], L_p	5.0	This work, MD modeling
	7.6	DA = 0.40 (Lamarque et al., 2005)
	4.5	(Schatz et al., 2003)
	5	(Rinaudo et al., 1993)
Molecule density [kg m^{-3}], ρ_p	1.82 ± 0.10 × 10^3	This work, MD modeling, no hydration
	1.49 ± 0.10 × 10^3	This work, MD modeling, hydration of 1 water molecule per protonated monomer
	1.35 ± 0.10 × 10^3	This work, MD modeling, with condensation of one Cl^- ion per one protonated monomer
	1.72 × 10^3	DA = 0.58, Errington et al. (1993)
Monomer volume [nm^3], ν_1	0.163	This work, no hydration, calculated as $\nu_1 = M_1/(\rho_p A_v)$
	0.200	This work, hydration
	0.221	Ion condensation
Monomer equivalent cylinder diameter [nm], d_c	0.672 ± 0.03	This work, no hydration, calculated as $d_c = (4\nu_1/\pi l_m)$
	0.744 ± 0.03	This work, hydration
	0.781 ± 0.03	This work, ion condensation
Extended chain diameter [nm], d_{ex}	0.662 ± 0.03	No hydration, calculated from contour length
	0.733 ± 0.03	This work, hydration
	0.769 ± 0.03	Ion condensation
Chain diameter [nm]	0.731 ± 0.03	No hydration, calculated from the average end-to-end Distance value for 0.01 M HCl
	0.809 ± 0.03	Hydration, 0.01 M HCl
	0.849 ± 0.03	Ion condensation, 0.01 M HCl

The agreement is even better when using the corresponding value relying only on the MD simulations of the shortest chain (0.474 nm) which is the most extensively sampled, providing probably the most accurate maximal extended chain value. Minor differences between theoretical predictions and the experimental data are expected due to the following factors: (i) deviations in the system composition with respect to the real systems (this includes both the necessary restrictions in the system size and the uncertain pattern of acetylation which does not necessarily correspond to the periodic one assumed in our MD simulations); (ii) sampling-inherent inaccuracies. The latter issue concerns mainly the persistence length as it cannot be determined using the enhanced-sampling metadynamics technique and is possible to be estimated only for sufficiently long chains (it was possible only for the longest chain in the case of presently studied systems) and, at the same time, is slowly converging variable. The presently estimated value of 5.0 nm is close to the lower limit of experimentally-inferred values, to the MD-relying value of 5 nm by Singhal et al. (Singhal et al., 2020) and persistence lengths calculated by Tsereteli and Grafmüller using the coarse-grained model and varying in the range of 6–9 nm (Tsereteli & Grafmüller, 2017). The latter work is also in line with our finding stating that the $GlcNH_3^+$-GlcNAc linkage is the most flexible one.

One should expect that the extrapolation of these results to a larger molar mass of chitosan furnishes useful data inaccessible for direct theoretical modeling because of excessive time of computations.

However, it is to remember that this only concerns chitosan samples of low dispersity.

3.2. Experimental characteristics of chitosan

Dry mass of chitosan powder was determined using classic thermogravimetry. The detailed protocol for these measurements can be found in Section 2.1 in Supporting Information. Such experiments showed that the water content in the chitosan sample was 8%.

Elemental composition of the chitosan sample, especially the C/N atomic ratio was determined using elemental analysis. Additionally, the presence of characteristic moieties and DA value were evaluated using Fourier transform infrared spectroscopy (FTIR).

It was 37% ± 3 and 39% ± 2, respectively. It was assumed that the distribution of the -NH_2 groups was quasi-periodic, as in theoretical modeling (see Fig. 1).

The calculation of DA, a spectrum of the chitosan sample and the most significant peaks visible in the spectrum, as well as their assignment to respective vibrations, were collected in Fig. S3 and Table S1, respectively.

The chitosan molecule density for various temperatures was determined by the dilution method according to the procedure described previously (Adamczyk et al., 2018). The primary results shown in Fig. S5 enabled to calculate the density from Eq. (5) using the slope of ρ_e/ρ_s vs. the mass fraction of chitosan in the solution, w_p analogously as for the theoretical modeling. In this way, one obtained $1.5 \pm 0.2 \times 10^3$ and $1.55 \pm 0.02 \times 10^3$ kg m^{-3} for the temperature of 298 K and 308 K, respectively. It is noteworthy here that the value of ρ_s determined at 298 K agrees with the result derived from MD modeling.

On the other hand, the molar mass of the chitosan sample determined by AF4-RI-MALS and MALDI-TOF/TOF MS was 412 and 346 kg mol^{-1} (kDa), respectively. These values differ significantly from the molar mass given by the producer, 50 to 190 kg mol^{-1} (average value 120 kg mol^{-1}), as determined by a viscosity method. However, such discrepancy is common for chitosan samples, where the molar mass derived for osmotic pressure measurements and MALS may differ in some cases by a factor up to 4.6 (Anthonsen et al., 1993). This is mainly attributed to the sample aggregation during the measurements. As shown in Ref. (Korchagina & Philippova, 2010) for the chitosan sample with M_p = 125 kDa, approx. 10% of chitosan chains are forming spherical aggregates characterized by an aggregation number of ca. 10.

Therefore, in this work except for the dynamic viscosity measurements, a few complementary methods were applied to derive information about the chitosan and conformations of its molecule in electrolyte solutions. Primarily, the dynamic light scattering (DLS) measurements were carried out yielding the diffusion coefficient of molecules from the light intensity autocorrelation function. The advantage of DLS method, compared to the static light scattering (MALS) is that no column separation of the sample is needed and that the signal is independent of the molecule shape. Additionally, macroion samples characterized by significant dispersity can be analyzed at a relatively low concentration range.

Extensive measurements discussed in Supporting Information enabled to determine the chitosan molecule diffusion coefficient as a function of pH varied between 2 and 6, for a fixed ionic strength of 0.01 M NaCl (see Fig. S9). Also, the dependence of the diffusion coefficient on the storage time was measured for various pHs in order to determine the chitosan solution stability. Finally, the dependence of the diffusion coefficient on the temperature, which varied between 293 and 323 K, was experimentally determined (see Fig. S10 part A). These data were converted to the molecule hydrodynamic diameter d_H using the Stokes-Einstein relationship (Einstein, 1908)

$$d_H = \frac{kT}{3\pi\eta D} \tag{6}$$

where: k is the Boltzmann constant, T is the absolute temperature, η is the dynamic viscosity of the electrolyte and D is the diffusion coefficient of the molecule derived from DLS.

It is revealed that there were two main fractions were present in the chitosan sample: the first one characterized by the hydrodynamic diameter of 19 ± 2 nm (number averaged) and the other exhibiting d_H = 40 ± 5 nm (also number averaged). Interestingly, the former value was fairly independent of pH and the storage time up to 72 h, which is illustrated in Fig. 5.

It is also observed that the hydrodynamic diameter at pH 2 (for the primary peak) decreased from 20 to 15 nm upon an increase of the temperature from 293 to 323 K (Fig. S10 part B).

It is interesting to compare the chitosan molecule hydrodynamic diameter derived from DLS with the diameter of an equivalent sphere d_s calculated as:

$$d_s = \left(\frac{6M_p}{\pi\rho_p N_A}\right)^{1/3} \tag{7}$$

For M_p = 50 kDa one obtains from Eq. (7) d_s = 4.7 nm. For M_p = 120 kDa (average value given by the producer), one obtains d_s = 6.3 nm. These values are significantly smaller than the DLS hydrodynamic diameter. This indicates that at an ionic strength of 0.01 M the chitosan molecule assumes a largely elongated shape, analogously as previously observed for other macroions (Adamczyk et al., 2018); (Michna et al., 2021). Therefore, it is reasonable to theoretically interpret the DLS results using the slender body hydrodynamics pertinent to the case where the length to width ratio (aspect ratio) of a molecule denoted by λ considerably exceeds unity (Brenner, 1974). For such a case the hydrodynamic diameter can be expressed in the following form (Mansfield & Douglas, 2008); (Adamczyk et al., 2012):

$$d_H = \frac{L_c}{c_1 ln2\lambda + c_2} = d_c\frac{\lambda}{c_1 ln2\lambda + c_2} \tag{8}$$

where L_c is the contour length of the molecule, c_1, c_2 are the dimensionless constants depending on the shape of the body and d_c is the molecule chain diameter.

For prolate spheroids one has $c_1 = 1$, $c_2 = 0$; for blunt cylinders: $c_1 = 1$, $c_2 = -0.11$; (Brenner, 1974) for linear chain of touching beads:$c_1 = 1$, $c_2 = 0.25$ and for a chain of beads forming a torus one has: $c_1 = 11/12$,

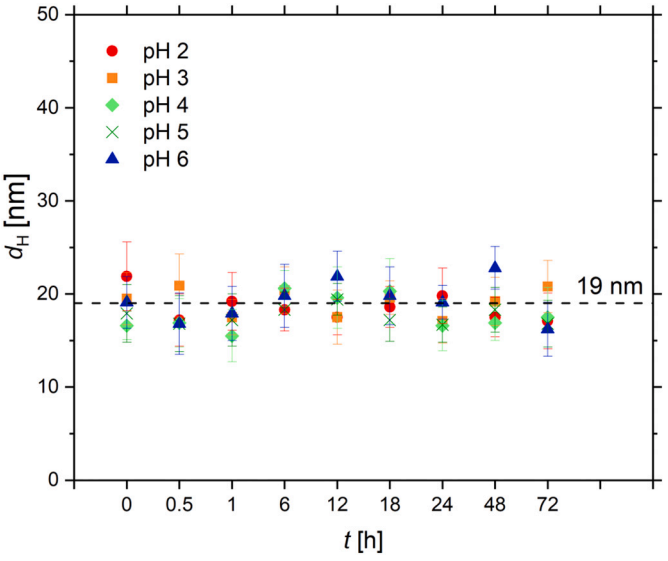

Fig. 5. The dependence of the hydrodynamic diameter of the chitosan molecule (first fraction) on pH and the storage time, I = 0.01 M; T = 298 K; bulk solution concentration 100 mg L^{-1}. The dashed line denotes the average value of d_H = 19 ± 2 nm.

$c_2 = 0.67$ (Adamczyk et al., 2006). Replacing the string of touching beads by a flexible cylinder of the same volume and length one obtains $c_1 = 1$, $c_2 = -0.45$ (linear chain) and $c_1 = 11/12$, $c_2 = 0.48$ (torus) (Adamczyk et al., 2006).

The L_c parameter appearing in Eq. (8) can be calculated as $l_m M_p/M_1$ using the monomer contour length l_m given in Table 1. For the extended chain (this corresponds to a low ionic strength limit) one has $l_m = 0.460$ nm, whereas for the 0.01 M ionic strength one has $l_m = 0.378$ nm. Using also the chain diameter of 0.733 nm (Table 1) one can calculate that for the molar mass of 50 kDa, where $L_c = L_{ex} = 280$ nm, the hydrodynamic diameter predicted from Eq.(8) is 21.9, 22.3 and 21.9 nm for spheroid, cylinder and torus, respectively. Analogously, for $I = 0.01$ M, where $L_c = 105$ nm and the chain diameter is 0.809 nm one obtains $d_H = 18.6$, 18.9 and 18.6 nm for spheroid, cylinder and torus. As can be seen, these values little depend on the molecule shape and agree within the error bound with the experimental value (DLS) 19 nm.

For the average molar mass of 120 kDa, $L_{ex} = 308$ nm, and $d_H = 45.7$, 46.5 and 46.3 nm for the spheroid, cylinder and torus, respectively, in the low ionic strength limit. Analogously, for 0.01 M ionic strength one obtains $d_H = 39.2$, 39.8 and 39.5 nm for the spheroid, cylinder and torus. Again, these values agree with the experimental hydrodynamic diameter derived from DLS (40 nm) for the second chitosan fraction. It is also worth mentioning that in Ref. (Korchagina & Philippova, 2010) a similar value of the hydrodynamic diameter 36 ± 4 nm was reported for an unaggregated chitosan sample having the molar mass of 125 kDa and DA = 5%.

Interestingly, for the straight cylinder conformation, the gyration radius becomes independent of the chitosan molecule diameter and can be calculated from the formula (Adamczyk et al., 2021)

$$R_g = \frac{L_c}{12^{1/2}} \tag{9}$$

Thus, for the molar mass of 50 kDa one can calculate from Eq. (9) that the gyration radius is 37 and 30.3 nm, in the limit of low ionic strength and for 0.01 M, respectively. Analogously, for the molar mass of 120 kDa, the gyration radius is 88.9 and 72.7 nm for these two cases, respectively.

Independently, the hydrodynamic diameter of chitosan molecules was determined as described above using OWLS, which yielded reproducible results for the low solution concentration of 5 mg L^{-1} where the interaction among chitosan molecules become negligible. Primarily, in these experiments, the adsorption kinetics of chitosan expressed as the mass coverage vs. the time dependence was determined under regulated flow rate (see Fig. S12). The hydrodynamic diameter obtained in this way at 0.01 M ionic strength was 38 ± 2 nm, which agrees with the theoretical data predicted for the average molar mass of the chitosan sample.

The hydrodynamic diameter data acquired above from DLS and OWLS can also be used to determine the electrokinetic charge of chitosan molecules, an essential parameter, which has not been before determined in the literature. This additionally requires the electrophoretic mobility of molecules μ_e (this parameter is the ratio of the molecule migration velocity to the applied electric field) which can be directly measured by the LDV method as described above. The dependence of μ_e on pH acquired at 0.01 M ionic strength and the temperature of 298 K is shown in Fig. 6. As can be noticed, the mobility attains a maximum value of 5.1 μm cm$(Vs)^{-1}$ at pH 2 and monotonically decreases to zero at pH ca. 8.5.

Using the experimental electrophoretic mobility μ_e and the hydrodynamic diameter one can determine the electrokinetic charge at the chitosan molecule by applying the Lorentz–Stokes relationship (Adamczyk et al., 2006); (Michna et al., 2017):

$$q_e = 3\pi\eta d_H \mu_e = \frac{kT}{D}\mu_e \tag{10}$$

Consequently, the number of elementary charges N_c per one molecule can be calculated as

$N_c = q_e/e$, where e is the elementary charge 1.602×10^{-19} C.

Eq. (10) is valid for an arbitrary charge distribution and the shape of molecules. However, its accuracy decreases for larger ionic strengths where the double-layer thickness $\kappa^{-1} = (\varepsilon kT/2e^2I)^{1/2}$ (where ε is the electric permittivity of the solvent) becomes comparable with the molecule diameter.

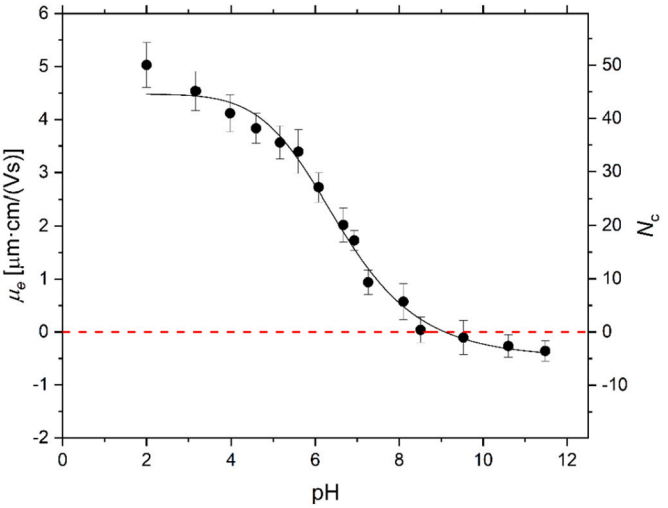

Fig. 6. The dependence of the electrophoretic mobility and the number of elementary charges per one chitosan molecule on pH. Measurement conditions: $I = 0.01$ M; $T = 298$ K; bulk solution concentration 300 mg L^{-1}. The solid line denotes the logistic fit of experimental results.

Using the experimental hydrodynamic diameter of 19 nm (for the molecule molar mass of 50 kDa) and the electrophoretic mobility data one obtains $N_c = 50$, 33 and 9 at pH 2, 5.6 and 7.3, respectively. The dependence of N_c on pH is graphically shown in Fig. 6. Analogously, for the average molar mass of 120 kDa where the hydrodynamic diameter is 40 nm one obtains $N_c = 105$, 69 and 19 at pH 2, 5.6 and 7.3, respectively. Considering that DP was 280 and 670 (for 50 and 120 kDa, respectively) and DA = 40% one can calculate that the electrokinetic charge at pH 2 amounts to 0.32 to 0.26 of the nominal charge (158 e and 402 e for 50 and 120 kDa, respectively). These results indicate that the molecule charge stemming from the protonated –NH_2 groups is significantly compensated by counterion accumulation in the diffuse part of the electric double-layer. This effect is well-known as the Manning ion condensation (Manning, 1979). It is also interesting to mention that such behaviour was previously reported for PDADMAC (Adamczyk et al., 2014), and PLL (Adamczyk et al., 2018) macroions.

Except for the electrokinetic charge, the electrophoretic mobility data allow to calculate the zeta potential, an important parameter controlling macromolecule interactions among themselves, i.e., their solution stability, and their interactions with interfaces, i.e., the adsorption kinetics and isotherms. The dependence of the chitosan molecule zeta potential on pH calculated from the electrophoretic mobility using the general Ohshima model is plotted in Fig. 7. The electrophoretic mobility, the zeta potential and the number of electrokinetic charges of the chitosan molecule at various pHs were presented in Table S4.

Furthermore, the dependences of zeta potential and the electrokinetic charge of the chitosan molecule on the temperature at pH = 2 for I = 0.01 M HCl were determined. The obtained results can be found in Fig. S11 and Table S5.

4. Viscosity measurements

Thorough characteristics of chitosan solutions were also acquired applying the viscosity method, widely used in the literature to determine

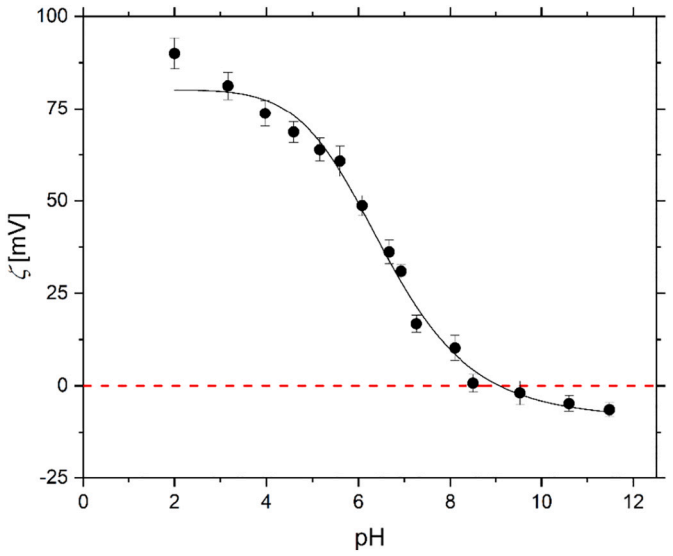

Fig. 7. Dependence of the zeta potential of the chitosan molecule on pH. Measurements conditions: $I = 0.01$ M; $T = 298$ K; bulk solution concentration 300 mg L^{-1}. The solid line denotes the logistic fit of experimental data.

the molar mass via the Mark-Houvink equation and other derivative parameters such as the chain conformation, persistence length, chain stiffness, etc. (Kasaai, 2007; Morris et al., 2009; Weinhold & Thöming, 2011) Primarily, in the measurements, the zero shear rate dynamic viscosity of dilute chitosan solution denoted as η_s was measured for various pHs and temperatures at a fixed ionic strength of 0.01 M. These primary results were expressed as the dependence of the normalized viscosity η_s/η_e (where η_e is the supporting electrolyte viscosity) on the chitosan volume fraction $\Phi_v = c_b/\rho_p$ rather than on the mass fraction as usually done in the literature.

Such dependencies of the normalized viscosity, η_s/η_e on the volume fraction Φ_v for various pHs, the temperature 298 K and $I = 0.01$ M are presented in Fig. 8. The dependencies of normalized viscosity on the volume fraction for various temperatures, at pH 2 are presented in Fig. S13.

It should be mentioned that dynamic viscosity measurements for

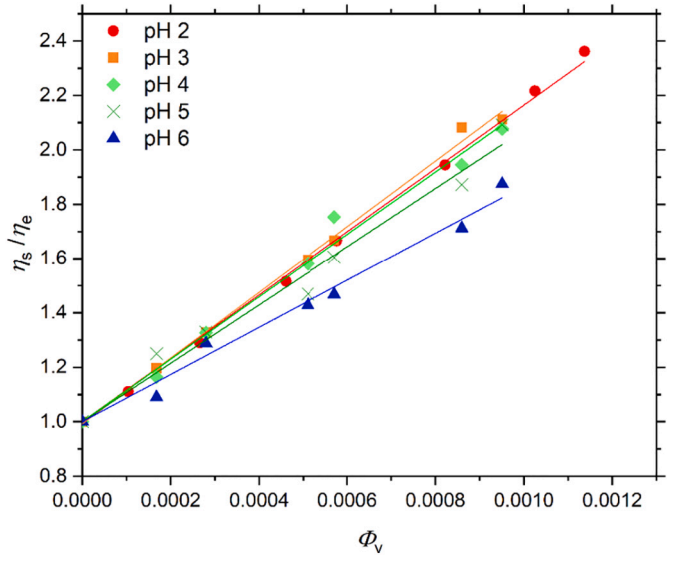

Fig. 8. Dependence of the normalized viscosity η_s/η_e on the volume fraction Φ_v of chitosan solutions at various pHs, $I = 0.01$ M, $T = 298$ K. The lines represent linear interpolation of the experimental data.

other ionic strength were less reproducible because of the instability of chitosan solutions. To be more precise, due to the lower solubility of chitosan in less concentrated solutions of HCl, the range of Φ_v presented in Fig. 8 is inaccessible under HCl concentration lower than 6×10^{-3} M, as determined experimentally. Additionally, the direct dilution of freshly prepared chitosan solution in 0.01 M HCl was applied to prepare chitosan solution of lower ionic strength. Unfortunately, this approach resulted in precipitation of chitosan. To the best of our knowledge, there is no available literature data concerning the dynamic viscosity of chitosan solutions characterized by ionic strength lower than 0.01 M.

The slopes of these dependencies give directly the experimental values of the intrinsic viscosity increment ν_{exp} (a dimensionless parameter) defined as

$$\nu_{exp} = [\eta]\rho_p \tag{11}$$

where $[\eta]$ is the usually defined intrinsic viscosity expressed as dL g^{-1}, therefore, having the dimension of a specific volume.

It is determined that ν_{exp} was practically independent of pH for the range 2–4 (see Fig. 8) assuming an average value of 1150 ± 50. This value is slightly lower for pH 5, attaining a value of 1070 ± 30. However, at pH 6, ν_{exp} markedly decreased assuming 860 ± 40 for the NaCl concentration of 0.01. Such large values of the viscosity increment, compared to the Einstein value of 2.5 pertinent to spherical (random coil) molecule conformation, unequivocally indicate that the chitosan molecule assumes largely extended conformation. This agrees with the above prediction derived from DLS and OWLS measurements.

The influence of the temperature on the viscosity increment at pH 2 and $I = 0.01$ M was also studied. The results shown in Fig. S14 and Table S6 confirmed that the increment decreased from 1150 ± 50 to 710 ± 30 for 293 and 323 K.

These viscosity increment data were interpreted in terms of theoretical results derived in Ref. (Brenner, 1974) within the framework of low Reynolds number hydrodynamics. In this work, the intrinsic viscosity increment was analytically calculated for prolate spheroids characterized by the elongation parameter λ up to 50. A broad range of the Peclet (*Pe*) number defining the significance of the hydrodynamic shear rate to the rotary diffusion coefficient of molecules was considered. In the limit of zero *Pe* number (corresponding to negligible shear rate) the exact numerical results obtained for $\lambda \gg 1$ were interpolated by the following analytical expression

$$\nu = c_{1\nu}\frac{\lambda^2}{ln2\lambda - 0.5} + c_{2\nu}\frac{\lambda^2}{ln2\lambda - 1.5} + c_\nu \tag{12}$$

where $c_{1\nu} = 3/15$, $c_{2\nu} = 1/15$ and c_ν is 8/5 for spheroids and 14/15 for blunt cylinders (Harding, 1995).

The precision of Eq. (12) is ca. 1% for $\lambda = 10$ and 0.2% for λ above 100.

However, one should underline that Eq. (12) is strictly valid for rigid bodies having regular shape such as prolate spheroids or cylinders of arbitrary cross-section area. No exact theoretical results were reported in the literature for flexible, worm-like, molecule shapes. However, there exist results for cyclic molecule chains approximated by strings of touching beads, either freely jointed or forming Gaussian rings, with a quasi-toroidal geometry (Bernal et al., 2002). The obtained results were expressed as the ratio of the intrinsic viscosity increment of the linear to the cyclic chains having the same number of beads, denoted as q_η. For the number of beads exceeding 20 (this corresponds to the λ parameter in the slender body nomenclature), it is shown that q_η was 0.60 ± 0.2. This result confirms that the increment of a flexible molecule bent to a form of a torus (a circle in the limit of large elongations) amounts to 60% of the molecule forming a fully expanded conformation. Therefore, it is reasonable to assume that any intermediate conformation such as example a semi-circle will produce even a smaller, about 20% change in the viscosity increments. By virtue of these results, one can calculate the limiting viscosity increment for a flexible molecule in the toroidal

conformation by multiplying the viscosity derived from Eq. (12) by the factor q_η. Theoretical results calculated in this way are given in Table 2 and compared with the experimental value determined in this work for 0.01 M ionic strength. As can be seen, the experimental value of 1150 ± 50 agrees with the theoretically predicted 1090, which was calculated for a straight molecule conformation and the molar mass of 50 kDa, whereas the toroidal conformation yields $\nu_c = 660$, i.e., significantly smaller. In contrast, for the average molar mass of 120 kDa, the theoretical values of the viscosity increment for the straight and toroidal conformation are 4590 and 2760, respectively, which significantly exceeds the experimental value. A plausible explanation of this discrepancy is the uncertainty in the molar mass determination, mainly caused by the presence of aggregates exhibiting significantly larger molar mass than the average value. As shown by Anthonsen et al. (Anthonsen et al., 1993) and Korchagina & Philippova (Korchagina & Philippova, 2010) such aggregates exhibit a compact molecule shape rather than largely elongated, pertinent to monomer molecules. As a result, although they shift the average molar mass to large values, they little contribute to the intrinsic viscosity. In order to test this hypothesis, some literature data acquired for well-defined experimental conditions are theoretically analyzed in terms of the hydrodynamic model using the molecule dimensions derived from this work from the MD modeling.

Errington et al. (Errington et al., 1993) carried out measurements for chitosan samples of various origins characterized by molar mass determined by the sedimentation equilibrium varying between 4.3 and 64 kDa and the acetylation degree of 58%. The ionic strength of the solution was 0.2 M and pH was 4.3. In contrast to other works, the density of the chitosan sample 1.72 g cm^{-3} was determined by the dilution method. The viscosity increment results shown in Table 2 indicate that an almost quantitative agreement with theoretical predictions is observed for the 28.9 and 64 kDa samples. However, for the low molar mass samples of 8.8 and 4.3 kDa, the experimental intrinsic viscosity increments were significantly larger than those predicted for a fully extended chain. This unusual behaviour can be attributed to the large uncertainty in the molar mass determination by the sedimentation equilibrium for low molar mass samples.

Anthonsen et al. (1993), performed systematic viscosity measurements for chitosan samples characterized by the molar mass (determined by osmotic pressure) varying between 15 and 310 kDa and acetylation degrees 60, 15 and 0%, respectively. Additionally, the influence of ionic strength changed between 1 and 0.013 M (at pH 5) was determined. In Table 2, the results obtained for DA = 15% and 0.013 M extrapolated to 0.01 M ionic strength are compared with the theoretical predictions derived from our model assuming $\rho_p = 1.72$ g cm^{-3} that corresponds to the experimental value determined by Errington et al. (1993). Considering the possible experimental error, a satisfactory

Table 2
Theoretical (derived from the slender body approach) and experimental values of the intrinsic viscosity increments of chitosan molecules in aqueous electrolyte solutions.

M_p [kDa]	DP [1]	L_{ext} R_g [nm]	λ_{ext} [1]	L_{01} R_g [nm]	λ_{01} [1]	ν_{ext} [1]	ν_{01} [1]	ν_c [1]	ν_{exp} [1]	Refs, Remarks
50	280	128 37.0	175	105 30.3	141	1610	1090	660	1150 ± 50	This work, DA = 40% $M_1 = 0.179$ kg mol^{-1} $\rho_p = 1.5$ g cm^{-3} pH 2–4, 0.01 M HCl $T = 298$ K
120	670	308 88.9	420	252 72.7	312	7910	4590	2760	1150	This work
125	748	344 99.3	469	282 81.4	348	9680	5600	3360	2100	Anthonsen et al. (1993) DA = 15%, $M_1 = 0.167$ kg mol^{-1} pH 5, 0.01 M NaCl $T = 295$ K, $\rho_p = 1.72$ g cm^{-3} (assumed)
98	587	270 77.9	368	222 64.1	274	6210	3630	2180	1900	
82	491	226 65.2	308	186 53.7	229	4490	2620	1570	1370	
78	467	215 62.1	293	176 50.8	218	4100	2400	1490	1250	
62	371	171 49.4	233	140 40.4	173	2700	1580	948	1030	
35	210	96.4 27.8	132	79.1 22.8	98.2	973	575	344	550	
120	714	329 95.0	448	270 77.9	333	8900	5170	3100	403	Tsaih and Chen (1999) DA = 17%, $M_1 = 0.168$ g mol^{-1} $\rho_p = 1.72$ g cm^{-3} (assumed) $T = 303$ K
78	464	214 61.8	292	176 50.8	217	4070	2380	1430	217	
64.1	347	160 46.2	218	132 38.1	162	2400	1400	842	1380	Errington et al. (1993) DA = 58%, $M_1 = 0.185$ g mol^{-1} $\rho_p = 1.72$ g cm^{-3} pH 4.3, 0.2 M NaCl $T = 298$ K
28.9	156	71.9 20.8	98.0	59.0 17.0	72.9	572	340	203	193	
8.8	47.6	21.9 6.3	29.9	18.0 5.2	22.2	74	45	27	115	
4.3	23.2	10.7 3.1	14.6	8.8 2.5	11.0	24	16	9.2	45	

$DP = M_p/M_1$ - degree of polymerization the molecule.
$L_{ext} = DPl_m$ - extended contour length of the molecule
$\lambda_{ext} = L_{ext}/d_{ex}$ - aspect ratio parameter.
$\lambda_{01} = \lambda_{ext}(d_{ex}/d_{01})^3$ - aspect ratio parameter for 0.01 M electrolyte
ν_{ext} = viscosity increment for fully extended chain, Eq. (12).
$\nu_{01} = f_v(\lambda_{01})$ - viscosity increment for a cylinder and a spheroid valid for $\lambda > 10$.
$\nu_c = C_c f_v(\lambda_{01})$ - viscosity increments for a cyclic molecule (Bernal et al., 2002) determined for 0.01 M electrolye.
$\nu_{exp} = [\eta]\rho_p$ - experimental viscosity increment.
$l_m = 0.460$ nm; $d_{ex} = 0.733$ nm; $l_{m01} = 0.378$ nm; $d_{01} = 0.809$ nm (Table 1).

agreement with theoretical predictions is evident for the molar mass range of 35 to 98 kDa. Only for the 125 kDa sample, the experimental intrinsic viscosity increment becomes markedly smaller than the theoretical value predicted for the toroidal conformation of the molecules. One can argue that this deviation can be attributed to the uncertainty in the molar mass determination by the osmotic pressure measurements. It may become significant for molar mass above 100 kDa given that the concentration of chitosan in the osmotic pressure measurements attained 6000 mg L^{-1}, increasing interactions among molecules, which may lead to aggregation.

The significant role of chitosan solutions aggregation creating uncertainty in molar mass determination is confirmed in other works. Thus, Tsaih and Chen (1999) performed systematic measurements of chitosan solution viscosity for samples characterized by molar mass determined by static light scattering varying between 78 and 914 kDa, and the acetylation degree of 17%, (at pH 2.18). The influence of ionic strength changed between 0.01 and 0.2 M at the temperature of 30 was investigated. In Table 2 the experimental results obtained for 78 and 120 kDa samples are compared with the theoretical predictions derived from our model assuming $\rho_p = 1.72$ g cm^{-3}. As can be inferred, the intrinsic viscosity increment for the molar mass of 120 kDa is almost eight times smaller than that theoretically predicted and more than four times smaller than the experimental value obtained by Anthonsen et al. (1993). For the molar mass of 78 kDa the increment is six times smaller than that obtained by Anthonsen for practically the same experimental conditions. The results obtained by Tsaih and Chen (1999) were interpreted in terms of the Mark-Houwink (MH) equation. For 0.01 M ionic strength, the a and K parameters were 0.715 and 5.48×10^{-4} dL g^{-1}, respectively.

5. Conclusions

Extensive MD modeling confirmed that the chitosan molecule exhibits in electrolyte solutions a flexible-rod shape showing no tendency to the formation of helical conformation. Several parameters of primary significance were theoretically calculated for the first time such as the monomer contour length, the hydrated chain diameter and the molecule density under different ionic strengths. Applying an extrapolation procedure these data enabled to calculate the contour length for chitosan molecules of various molar masses and the molecule length to diameter ratio. Considering that the latter parameter assumes large values, the molecule hydrodynamic diameter, gyration radius and the intrinsic viscosity increments were calculated by applying the slender body hydrodynamics. It was predicted that the hydrodynamic diameter for straight and bent molecule conformation was practically equal, whereas the increment decreased by ca. 40% for the toroidal molecule conformation. These theoretical results allowed to quantitatively interpret experimental measurements, where the diffusion coefficient, the hydrodynamic diameter, the electrophoretic mobility and the intrinsic viscosity increment of the chitosan molecule were determined at a broad range of pH and the temperature. A satisfactory agreement was attained considering the sample dispersity.

Additionally, a thorough analysis of extensive literature data acquired under well-defined experimental conditions confirmed the utility of the hydrodynamic model developed in this work for predicting intrinsic viscosity of lower molar mass chitosan solutions.

It is argued that besides significance for basic science as reference data, the obtained results can be exploited for the optimization of procedures for macroion film formation at various substrates often used as efficient supports for bioparticle immobilization.

CRediT authorship contribution statement

Dawid Lupa: Investigation, Methodology, Visualization, Writing – original draft, Writing – review & editing. **Wojciech Płaziński:** Investigation, Methodology, Visualization, Writing – original draft, Writing – review & editing. **Aneta Michna:** Investigation, Methodology, Writing – review & editing, Funding acquisition. **Monika Wasilewska:** Investigation, Methodology, Writing – original draft. **Paweł Pomastowski:** Investigation, Methodology, Writing – original draft. **Adrian Gołębiowski:** Investigation, Methodology, Writing – original draft. **Bogusław Buszewski:** Conceptualization, Writing – review & editing, Data curation. **Zbigniew Adamczyk:** Conceptualization, Writing – original draft, Writing – review & editing, Supervision.

Declaration of competing interest

The authors declare that they have no known competing financial interests or personal relationships that could have appeared to influence the work reported in this paper.

Acknowledgments

This work was financially supported by the National Science Centre, Poland, Opus Project, UMO-2018/31/B/ST8/03277 and partially by the Statutory activity of the J. Haber Institute of Catalysis and SurfaceChemistry PAS (advanced calculation for interpretation of experimental data).

Paweł Pomastowski, Adrian Gołębiowski and Bogusław Buszewski are members of Toruń Center of Excellence "Towards Personalized Medicine" operating under Excellence Initiative-Research University.

Appendix A. Supplementary data

Supplementary data to this article can be found online at https://doi.org/10.1016/j.carbpol.2022.119676.

References

Abraham, M. J., Murtola, T., Schulz, R., Páll, S., Smith, J. C., Hess, B., & Lindahl, E. (2015). GROMACS: High performance molecular simulations through multi-level parallelism from laptops to supercomputers. *SoftwareX, 1–2*, 19–25. https://doi.org/10.1016/j.softx.2015.06.001

Adamczyk, Z., Bratek, A., Jachimska, B., Jasiński, T., & Warszyński, P. (2006). Structure of poly(acrylic acid) in electrolyte solutions determined from simulations and viscosity measurements. *Journal of Physical Chemistry B, 110*(45), 22426–22435. https://doi.org/10.1021/jp063981w

Adamczyk, Z., Cichocki, B., Ekiel-Jeżewska, M. L., Słowicka, A., Wajnryb, E., & Wasilewska, M. (2012). Fibrinogen conformations and charge in electrolyte solutions derived from DLS and dynamic viscosity measurements. *Journal of Colloid and Interface Science, 385*(1), 244–257. https://doi.org/10.1016/j.jcis.2012.07.010

Adamczyk, Z., Jamrozy, K., Batys, P., & Michna, A. (2014). Influence of ionic strength on poly(diallyldimethylammonium chloride) macromolecule conformations in electrolyte solutions. *Journal of Colloid and Interface Science, 435*, 182–190. https://doi.org/10.1016/j.jcis.2014.07.037

Adamczyk, Z., Morga, M., Kosior, D., & Batys, P. (2018). Conformations of poly-l-lysine molecules in electrolyte solutions: Modeling and experimental measurements. *Journal of Physical Chemistry C, 122*(40), 23180–23190. https://doi.org/10.1021/acs.jpcc.8b07606

Adamczyk, Z., Batys, P., Płaziński, W., Morga, M., Lupa, D., & Michna, A. (2021). Macroion molecule properties from slender body hydrodynamics. *Polymers for Advanced Technologies, 32*(10), 3900–3908. https://doi.org/10.1002/PAT.5319

Anthonsen, M. W., Vårum, K. M., & Smidsrød, O. (1993). Solution properties of chitosans: Conformation and chain stiffness of chitosans with different degrees of N-acetylation. *Carbohydrate Polymers, 22*(3), 193–201. https://doi.org/10.1016/0144-8617(93)90140-Y

Bano, I., Arshad, M., Yasin, T., & Ghauri, M. A. (2019). Preparation, characterization and evaluation of glycerol plasticized chitosan/PVA blends for burn wounds. *International Journal of Biological Macromolecules, 124*, 155–162. https://doi.org/10.1016/j.ijbiomac.2018.11.073

Barducci, A., Bussi, G., & Parrinello, M. (2008). Well-tempered metadynamics: A smoothly converging and tunable free-energy method. *Physical Review Letters, 100*(2), Article 020603. https://doi.org/10.1103/PhysRevLett.100.020603

Bernal, J. M. G., Tirado, M. M., Freire, J. J., & García De La Torre, J. (2002). Monte Carlo calculation of hydrodynamic properties of cyclic polymers in ideal solution. *Macromolecules, 23*(13), 3357–3362. https://doi.org/10.1021/MA00215A024

Berth, G., & Dautzenberg, H. (2002). The degree of acetylation of chitosans and its effect on the chain conformation in aqueous solution. *Carbohydrate Polymers, 47*(1), 39–51. https://doi.org/10.1016/S0144-8617(00)00343-X

Boardman, S. J., Lad, R., Green, D. C., & Thornton, P. D. (2017). Chitosan hydrogels for targeted dye and protein adsorption. *Journal of Applied Polymer Science, 44846*. https://doi.org/10.1002/app.44846

Brenner, H. (1974). Rheology of a dilute suspension of axisymmetric brownian particles. *International Journal of Multiphase Flow, 1*(2), 195–341. https://doi.org/10.1016/0301-9322(74)90018-4

Bussi, G., Donadio, D., & Parrinello, M. (2007). Canonical sampling through velocity rescaling. *The Journal of Chemical Physics, 126*(1), Article 014101. https://doi.org/10.1063/1.2408420

Chien, R. C., Yen, M. T., & Mau, J. L. (2016). Antimicrobial and antitumor activities of chitosan from shiitake stipes, compared to commercial chitosan from crab shells. *Carbohydrate Polymers, 138*, 259–264. https://doi.org/10.1016/j.carbpol.2015.11.061

Cölfen, H., Berth, G., & Dautzenberg, H. (2001). Hydrodynamic studies on chitosans in aqueous solution. *Carbohydrate Polymers, 45*(4), 373–383. https://doi.org/10.1016/S0144-8617(00)00269-1

Czechowska-Biskup, R., Wojtasz-Pająk, A., Sikorski, J., Henke, A., Ulański, P., & Rosiak, J. M. (2007). Aqueous solutions of hydrochloric acid as simple solvents of chitosan for viscosity- and light-scattering-based molecular weight determination. *Polish Chitin Society*, 87–94.

Darden, T., York, D., & Pedersen, L. (1998). Particle mesh Ewald: An N·log(N) method for Ewald sums in large systems. *The Journal of Chemical Physics, 98*(12), 10089. https://doi.org/10.1063/1.464397

Earl, D. J., & Deem, M. W. (2005). Parallel tempering: Theory, applications, and new perspectives. *Physical Chemistry Chemical Physics, 7*(23), 3910–3916. https://doi.org/10.1039/B509983H

Einstein, A. (1908). Elementare theorie der brownschen 1) bewegung. *Zeitschrift für Elektrochemie und Angewandte Physikalische Chemie, 14*(17), 235–239. https://doi.org/10.1002/bbpc.19080141703

Errington, N., Harding, S. E., Vårum, K. M., & Illum, L. (1993). Hydrodynamic characterization of chitosans varying in degree of acetylation. *International Journal of Biological Macromolecules, 15*(2), 113–117. https://doi.org/10.1016/0141-8130(93)90008-A

González-Espinosa, Y., Sabagh, B., Moldenhauer, E., Clarke, P., & Goycoolea, F. M. (2019). Characterisation of chitosan molecular weight distribution by multi-detection asymmetric flow-field flow fractionation (AF4) and SEC. *International Journal of Biological Macromolecules, 136*, 911–919. https://doi.org/10.1016/j.ijbiomac.2019.06.122

Guvench, O., Mallajosyula, S. S., Raman, E. P., Hatcher, E., Vanommeslaeghe, K., Foster, T. J., Jamison, F. W., & Mackerell, A. D. (2011). CHARMM additive all-atom force field for carbohydrate derivatives and its utility in polysaccharide and carbohydrate À protein modeling. *Journal of Chemical Theory and Computation, 7*(10), 3162–3180. https://doi.org/10.1021/ct200328p

Harding, S. E. (1995). On the hydrodynamic analysis of macromolecular conformation. *Biophysical Chemistry, 55*(1–2), 69–93. https://doi.org/10.1016/0301-4622(94)00143-8

Harding, S. E., Tombs, M. P., Adams, G. G., Paulsen, B. S., Inngjerdingen, K. T., & Barsett, H. (2017). Marine polysaccharides. In S. E. Harding, M. P. Tombs, G. G. Adams, B. S. Paulsen, K. T. Inngjerdingen, & H. Barsett (Eds.), *An introduction to polysaccharide biotechnology* (2nd ed., pp. 153–192). Taylor & Francis Group.

Hasegawa, M., Isogai, A., & Onabe, F. (1994). Molecular mass distribution of chitin and chitosan. *Carbohydrate Research, 262*(1), 161–166. https://doi.org/10.1016/0008-6215(94)84013-X

Hess, B. (2008). P-LINCS: A parallel linear constraint solver for molecular simulation. *Journal of Chemical Theory and Computation, 4*(1), 116–122. https://doi.org/10.1021/ct700200b

Hockney, R. (1970). The potential calculation and some applications. In B. Alder, S. Fernbach, & M. Rotenberg (Eds.), *Methods in computational physics* (pp. 135–211).

Jorgensen, W. L., Chandrasekhar, J., Madura, J. D., Impey, R. W., & Klein, M. L. (1998). Comparison of simple potential functions for simulating liquid water. *The Journal of Chemical Physics, 79*(2), 926. https://doi.org/10.1063/1.445869

Kaczmarek, M. B., Struszczyk-Swita, K., Li, X., Szczęsna-Antczak, M., & Daroch, M. (2019). Enzymatic modifications of chitin, chitosan, and chitooligosaccharides. *Frontiers in Bioengineering and Biotechnology, 7*, 243. https://doi.org/10.3389/fbioe.2019.00243

Kasaai, M. R. (2007). Calculation of Mark–Houwink–Sakurada (MHS) equation viscometric constants for chitosan in any solvent–temperature system using experimental reported viscometric constants data. *Carbohydrate Polymers, 68*(3), 477–488. https://doi.org/10.1016/j.carbpol.2006.11.006

Korchagina, E. V., & Philippova, O. E. (2010). Multichain aggregates in dilute solutions of associating polyelectrolyte keeping a constant size at the increase in the chain length of individual macromolecules. *Biomacromolecules, 11*(12), 3457–3466. https://doi.org/10.1021/bm100990u

Lamarque, G., Lucas, J. M., Viton, C., & Domard, A. (2005). Physicochemical behavior of homogeneous series of acetylated chitosans in aqueous solution: Role of various structural parameters. *Biomacromolecules, 6*(1), 131–142. https://doi.org/10.1021/bm0496357

Manning, G. S. (1979). Counterion binding in polyelectrolyte theory. *Accounts of Chemical Research, 12*(12), 443–449. https://doi.org/10.1021/ar50144a004

Mansfield, M. L., & Douglas, J. F. (2008). Transport properties of rodlike particles. *Macromolecules, 41*(14), 5422–5432. https://doi.org/10.1021/ma702839w

Meng, X., Liu, H., Dong, X., Wang, Q., Xia, Y., & Hu, X. (2022). A soft Pickering emulsifier made from chitosan and peptides endows stimuli-responsiveness, bioactivity and biocompatibility to emulsion. *Carbohydrate Polymers, 277*, Article 118768. https://doi.org/10.1016/j.carbpol.2021.118768

Michna, A., Adamczyk, Z., Sofińska, K., & Matusik, K. (2017). Monolayers of poly(amido amine) dendrimers on mica – In situ streaming potential measurements. *Journal of Colloid and Interface Science, 485*, 232–241. https://doi.org/10.1016/j.jcis.2016.09.007

Michna, A., Pomorska, A., Nattich-Rak, M., Wasilewska, M., & Adamczyk, Z. (2020). Hydrodynamic solvation of poly(amido amine) dendrimer monolayers on silica. *Journal of Physical Chemistry C, 124*, 17684–17695. https://doi.org/10.1021/acs.jpcc.0c04638

Michna, A., Płaziński, W., Lupa, D., Wasilewska, M., & Adamczyk, Z. (2021). Carrageenan molecule conformations and electrokinetic properties in electrolyte solutions: Modeling and experimental measurements. *Food Hydrocolloids, 121*, Article 107033. https://doi.org/10.1016/j.foodhyd.2021.107033

Miyamoto, S., & Kollman, P. A. (1992). Settle: An analytical version of the SHAKE and RATTLE algorithm for rigid water models. *Journal of Computational Chemistry, 13*(8), 952–962. https://doi.org/10.1002/jcc.540130805

Morris, G. A., Castile, J., Smith, A., Adams, G. G., & Harding, S. E. (2009). Macromolecular conformation of chitosan in dilute solution: A new global hydrodynamic approach. *Carbohydrate Polymers, 76*(4), 616–621. https://doi.org/10.1016/j.carbpol.2008.11.025

Ohshima, H. (2012). Electrophoretic mobility of charged particles. In H. Ohshima (Ed.), *Electrical phenomena at interfaces and biointerfaces: Fundamentals and applications in nano-, bio-, and environmental sciences* (1st ed., pp. 35–49). John Wiley & Sons Inc.

Park, S., Lee, J., Qi, Y., Kern, N. R., Lee, H. S., Jo, S., Joung, I., Joo, K., Lee, J., & Im, W. (2019). CHARMM-GUI Glycan Modeler for modeling and simulation of carbohydrates and glycoconjugates. *Glycobiology, 29*(4), 320–331. https://doi.org/10.1093/glycob/cwz003

Parrinello, M., & Rahman, A. (1981). Polymorphic transitions in single crystals: A new molecular dynamics method. *Journal of Applied Physics, 52*(12), 7182–7190. https://doi.org/10.1063/1.328693

Patrulea, V., Ostafe, V., Borchard, G., & Jordan, O. (2015). Chitosan as a starting material for wound healing applications. *European Journal of Pharmaceutics and Biopharmaceutics, 97*, 417–426. https://doi.org/10.1016/j.ejpb.2015.08.004

Pini, N. I. P., Lima, D. A. N. L., Luka, B., Ganss, C., & Schlueter, N. (2020). Viscosity of chitosan impacts the efficacy of F/Sn containing toothpastes against erosive/abrasive wear in enamel. *Journal of Dentistry, 92*, Article 103247. https://doi.org/10.1016/j.jdent.2019.103247

Raguzzoni, J. C., Delgadillo, I., & Lopes da Silva, J. A. (2016). Influence of a cationic polysaccharide on starch functionality. *Carbohydrate Polymers, 150*, 369–377. https://doi.org/10.1016/j.carbpol.2016.05.024

Rajabi, M., McConnell, M., Cabral, J., & Ali, M. A. (2021). Chitosan hydrogels in 3D printing for biomedical applications. *Carbohydrate Polymers, 260*, Article 117768. https://doi.org/10.1016/j.carbpol.2021.117768

Rinaudo, M., Milas, M., & Dung, P. L. (1993). Characterization of chitosan. Influence of ionic strength and degree of acetylation on chain expansion. *International Journal of Biological Macromolecules, 15*(5), 281–285. https://doi.org/10.1016/0141-8130(93)90027-J

Saha, D., & Bhattacharya, S. (2010). Hydrocolloids as thickening and gelling agents in food: A critical review. *Journal of Food Science and Technology, 47*(6), 587–597. https://doi.org/10.1007/s13197-010-0162-6

Schatz, C., Viton, C., Delair, T., Pichot, C., & Domard, A. (2003). Typical physicochemical behaviors of chitosan in aqueous solution. *Biomacromolecules, 4*(3), 641–648. https://doi.org/10.1021/bm025724c

Singhal, A., Schneible, J. D., Lilova, R. L., Hall, C. K., Menegatti, S., & Grafmüller, A. (2020). A multiscale coarse-grained model to predict the molecular architecture and drug transport properties of modified chitosan hydrogels. *Soft Matter, 16*(47), 10591–10610. https://doi.org/10.1039/d0sm01243b

Soares, L.d. S., Perim, R. B., de Alvarenga, E. S., Guimarães, L.d. M., Teixeira, A. V. N. d. C., Coimbra, J. S.d. R., & de Oliveira, E. B. (2019). Insights on physicochemical aspects of chitosan dispersion in aqueous solutions of acetic, glycolic, propionic or lactic acid. *International Journal of Biological Macromolecules, 128*(1), 140–148. https://doi.org/10.1016/j.ijbiomac.2019.01.106

Suo, H., Zhang, J., Xu, M., & Wang, L. (2021). Low-temperature 3D printing of collagen and chitosan composite for tissue engineering. *Materials Science and Engineering C, 123*, Article 111963. https://doi.org/10.1016/j.msec.2021.111963

Tribello, G. A., Bonomi, M., Branduardi, D., Camilloni, C., & Bussi, G. (2014). PLUMED 2: New feathers for an old bird. *Computer Physics Communications, 185*(2), 604–613. https://doi.org/10.1016/j.cpc.2013.09.018

Tsaih, M. L., & Chen, R. H. (1999). Effects of ionic strength and pH on the diffusion coefficients and conformation of chitosans molecule in solution. *Journal of Applied Polymer Science, 73*(10), 2041–2050. https://doi.org/10.1002/(SICI)1097-4628(19990906)73:10<2041::AID-APP22>3.0.CO;2-T

Tsereteli, L., & Grafmüller, A. (2017). An accurate coarse-grained model for chitosan polysaccharides in aqueous solution. *PLoS ONE, 12*(7), Article e0180938. https://doi.org/10.1371/journal.pone.0180938

Vakili, M., Rafatullah, M., Salamatinia, B., Abdullah, A. Z., Ibrahim, M. H., Tan, K. B., Gholami, Z., & Amouzgar, P. (2014). Application of chitosan and its derivatives as adsorbents for dye removal from water and wastewater: A review. *Carbohydrate Polymers, 113*, 115–130. https://doi.org/10.1016/j.carbpol.2014.07.007

Wan Ngah, W. S., Teong, L. C., & Hanafiah, M. A. K. M. (2011). Adsorption of dyes and heavy metal ions by chitosan composites: A review. *Carbohydrate Polymers, 83*(4), 1446–1456. https://doi.org/10.1016/j.carbpol.2010.11.004

Wang, W., Bo, S., Li, S., & Qin, W. (1991). Determination of the Mark-Houwink equation for chitosans with different degrees of deacetylation. *International Journal of Biological Macromolecules, 13*(5), 281–285. https://doi.org/10.1016/0141-8130(91)90027-R

Wardy, W., Pujols Martínez, K. D., Xu, Z., No, H. K., & Prinyawiwatkul, W. (2014). Viscosity changes of chitosan solution affect physico-functional properties and

consumer perception of coated eggs during storage. *LWT - Food Science and Technology, 55*(1), 67–73. https://doi.org/10.1016/j.lwt.2013.07.013

Wasilewska, M., Adamczyk, Z., Pomorska, A., Nattich-Rak, M., & Sadowska, M. (2019). Human serum albumin adsorption kinetics on silica: Influence of protein solution stability. *Langmuir, 35*(7), 2639–2648. https://doi.org/10.1021/acs.langmuir.8b03266

Weinhold, M. X., & Thöming, J. (2011). On conformational analysis of chitosan. *Carbohydrate Polymers, 84*(4), 1237–1243. https://doi.org/10.1016/j.carbpol.2011.01.011